The International Journal of Advanced Manufacturing Technology (2024) 134:2897–2919
https://doi.org/10.1007/s00170-024-14257-5

ORIGINAL ARTICLE

Influence of turning parameters on residual stresses and roughness of 42CrMo4 + QT

Diego Díaz-Salamanca[1] · Miguel Muñiz-Calvente[1] · Pejman Ebrahimzadeh[2] · Iñigo Llavori[3] · Alaitz Zabala[3] · Pablo Pando[1] · Carlos Suárez Álvarez[1] · Inés Fernández-Pariente[2] · Miren Larrañaga[3] · Jan Papuga[4]

Received: 19 April 2024 / Accepted: 7 August 2024 / Published online: 27 August 2024
© The Author(s) 2024

Abstract

Residual stresses and surface roughness have been recognized to play a critical role in the fatigue strength of metal components. Machining processes can induce different roughness and residual stress conditions depending on the parameters used in the process. Therefore, it is essential to develop knowledge that helps to predict the residual stresses and roughness that would be obtained from different machining conditions. Due to the growing interest from the industry in the use of 42CrMo4 steel because of its excellent mechanical properties, the main objective of this work is to establish two phenomenological models to accurately predict the residual stress and roughness values in turned specimens of this material. The models are derived from data of four process variables: (a) insert tip radius; (b) feed rate; (c) cutting speed; and (d) depth of cut. For this purpose, a wide experimental campaign has been developed, which includes the machining of 68 specimens under various cutting scenarios, and their subsequent measurement of residual stresses and roughness. Once the experimental data were obtained, the response surface method based on the central composite design was used to fit the models, obtaining a correlation index R^2 higher than 0.9 in both cases. In this article, it is concluded that feed rate and insert radius have a greater effect on the residual stress and roughness obtained, while cutting speed and depth of cut have a lesser impact on the results. It is hoped that the findings will establish a groundwork for the machining of this material type, ensuring controlled conditions of residual stress and roughness.

Keywords Turning process · Roughness · Residual stresses · Response surface methodology

Nomenclatures

RSM	Response surface methodology
CCD	Central composite design
CNC	Computer numerical control
f_n	Feed rate
V_C	Cutting speed
a_p	Depth of cut
R	Insert radius
E	Elastic modulus
υ	Poisson's modulus
hkl	Diffraction plane
d	Interplanar distance
ψ	Tilt angle
ϕ	Scattering angle
R_a	Average roughness
λ_c	Selected cut-off length
σ_{RSL}	Longitudinal residual stress
R_m	Ultimate tensile strength
HRb	Rockwell B hardness
r	Pearson correlation coefficient

✉ Diego Díaz-Salamanca
diazsdiego@uniovi.es

[1] Dep. of Construction and Manufacturing Engineering, Univesity of Oviedo, Gijón, Spain

[2] Dep. of Materials Sciences and Metallurgical Engineering, Univesity of Oviedo, Gijón, Spain

[3] Faculty of Engineering, Mechanics and Industrial Production, Mondragon Unibertsitatea, Mondragon, Spain

[4] Faculty of Mechanical Engineering, Czech Technical University in Prague, Prague, Czechia

1 Introduction

Different standards, such as DIN 50100 [1] / ASTM E466-15 [2] / ISO 1099 [3] establish the conditions for fatigue life characterization testing of metallic materials. Among the geometries available in these standards, cylindrical cross-sections are the most widely used, since stress concentrators and sharp corners are reduced. For this reason, the turning process, used to manufacture the cylindrical specimens,

takes on special relevance in the characterization of fatigue life. Nevertheless, turning processes invoke two effects that can largely condition the characterization of fatigue life: surface roughness and residual stresses.

On the one hand, the optimal cutting conditions in the last machining passes must be studied to mitigate the residual stresses, since tensile residual stresses can decrease fatigue life, while compressive residual stresses can increase it [4]. Both scenarios are inadvisable during a material characterization phase, where material properties should be established without the effect of residual stresses.

The residual stresses generated during the machining process and the magnitude of these stresses depend mainly on the cutting conditions and on the material under study. During turning, specimens are subjected to thermal gradients and heterogeneous plastic deformations, which conduce to the generation of thermo-mechanical loads, hence inducing residual stresses in the specimens [5, 6]. The influence of the different turning parameters (tool tip radius, cutting speed, feed rate, and depth of cut, among others) has been studied in previous works [7, 8]. Among these parameters, depth of cut is found to have the least impact on residual stresses, while cutting speed, feed rate, and tool tip radius are the most influential parameters [8, 9]. However, there is still no clear consensus regarding the effect of each of these three parameters. Although most authors agree that an increase in feed rate results in an increase in axial residual stresses and hence in a decrease in fatigue life, [10, 11], other works reveal that an increase in feed rate leads to an increase in compressive residual stresses [11]. Unfortunately, until this date, there are no physical models that relate the machining parameters to the residual stresses generated, so it is necessary to resort to experimentation and the fitting of empirical models to solve the problem.

On the other hand, a high surface roughness has a negative influence on the fatigue life, shortening it significantly. In addition, other properties such as tribological behavior or corrosion resistance are affected by the variation of surface roughness [12]. Cutting conditions play a critical role on the surface roughness of the workpiece, mainly cutting speed, feed rate, depth of cut, and tool radius [13, 14]. In the literature, predictive analytical equations to estimate the roughness as a function of the turning conditions (depth, feed, and tip radius) can be found [15]. However, these equations need to be revised for extreme cutting conditions, where feeds or depths may be outside the usual range of application of the tool, and which may be necessary to adopt to achieve low residual stresses. In these circumstances, characterized by the high plasticity of the material, these analytical relationships may not be applicable.

In the turning process, the presence of residual stresses alongside surface roughness significantly influences the fatigue endurance and mechanical properties of the final product. Therefore, achieving optimal performance depends heavily on the precise adjustment of turning parameters. However, conventional experiments which are based on trial-and-error techniques are not only expensive but also frequently fail to yield the desired results. Hence, there is a pressing need for more efficient estimation and optimization strategies to enhance the durability and overall quality of the machined components. To overcome this, researchers now utilize analytical and mathematical models, providing a more precise and efficient path to estimation and optimization. Response surface methodology (RSM) emerges as a powerful tool in this regard, streamlining experimentation and facilitating the exploration of variable interactions. Its adaptability shines through diverse applications, such as enhancing formability in friction stir welded blanks [16], refining laser micromachining techniques [17], and optimizing turning parameters [18]. These examples underscore RSM's effectiveness across various experimental scenarios, providing a structured framework for process analysis and optimization across different domains.

The main objective of this paper is to establish analytical relationships between the parameters of the turning process, residual stresses, and surface roughness for a 42CrMo4 quenched and tempered steel (in the following referred to as 42CrMo4 + QT). For this purpose, the effect of the main turning parameters (cutting speed, feed rate, tool tip radius, and depth of cut) on residual stress and surface roughness has been studied. The residual stresses were measured by means of an X-ray diffractometer, while a confocal microscope was used to evaluate the surface roughness. The experimental campaign has been designed employing a central composite design (CCD) of experiments, one of the most widely used methods within RSM. Thanks to the use of this design of experiments, it was possible to obtain acceptable information to build a predictive model, which allows to estimate the roughness and residual stress as a function of those turning parameters.

The manuscript is structured as follows. Firstly, a section devoted to introducing the methods and material used in this research is presented, which includes a description of the material selected, the geometry of the samples, the machining conditions, the design of experiments, the manufacturing, the measurement procedures used for both residual stress and roughness and the evaluation of the results. Subsequently, the results obtained are presented in detail. After that, the methodology to derive the phenomenological models is explained and the results obtained from the model are critically discussed. Finally, the main conclusions of this work are highlighted.

2 Methods and material

This section is intended to explain the experimental procedure followed in the development of this work according to the flowchart shown in Fig. 1. First, the properties of the material under study are introduced. Next, the dimensions of the specimens that will be manufactured are presented.

The ranges of cutting conditions have been selected and the design of experiments that establish the different combinations of machining parameters to be used have been presented. After that, the roughness and residual stress measurement methods are explained in detail. Finally, the results evaluations through the RSM are described.

2.1 Material selection

The material used in this work was a quenched and tempered 42CrMo4 steel. The mechanical properties of this medium carbon ferritic-pearlitic steel include its high resistance to fatigue and impact. These properties, together with its high machinability, make it suitable for a wide range of applications in the automotive, aeronautical, and energy industries. Some of these applications include the manufacture of high-strength components such as shafts, gears, screws, or pins, thanks to their excellent mechanical properties [19, 20].

For the development of this experimental campaign, a 35-mm diameter 42CrMo4 + QT steel round bar, obtained from the same casting T46157/2020 produced by TŘINECKÉ ŽELEZÁRNY, a.s., was used to reduce the existing inhomogeneities between the different machined specimens. The chemical composition and the mechanical properties of the material are shown in Table 1 and Table 2, respectively.

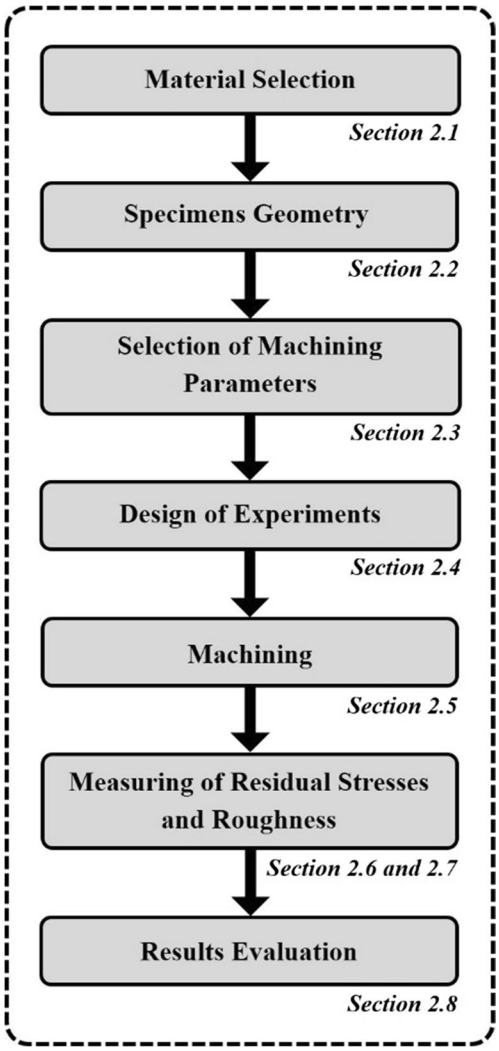

Fig. 1 Experimental campaign flowchart

2.2 Samples geometry

The geometry of the specimens selected to perform this research is shown in Fig. 2. This geometrical configuration was selected according to the following requirements. The first and most decisive of these was to facilitate the surface characterization of the specimens, which implied the need to machine a region of constant cross-section. The second requirement was to obtain a region in which the cutting conditions were homogeneous.

2.3 Selection of machining parameters

The main parameters governing the turning process are shown in Fig. 3. The crucial machining parameters utilized here are as follows: feed rate, cutting speed, depth of cut, and insert radius. These four variables were selected to study their impact on roughness and residual stress measured in the final specimens. The range in which each parameter will be tested is presented in the next paragraphs.

Regarding cutting speed, it is conditioned by the capacity of the lathe used for the manufacture of the specimens and by the diameter of the samples. In this research, a JATOR TAJ-42 computer numerical control (CNC) lathe was used, whose technical specifications can be seen in Table 3. Taking this into consideration, the range of the cutting speeds was defined between 76 and 200 m/min.

Table 2 Mechanical properties of 42CrMo4 + QT

Mechanical properties	Value
Yield stress (MPa)	1001.5
Tensile stress (MPa)	1097
Hardness (HV10)	310–370 (see [21])
Impact toughness (KV)	83.5 at 20 °C

Table 1 Chemical composition of 42CrMo4 + QT steel used (wt. %)

C	Mn	Si	P	S	Cu	Cr	Ni	Al	Mo	V	Ti	Sn
0.42	0.64	0.21	0.013	0.009	0.02	1.04	0.06	0.026	0.185	0.006	0.0013	0.003

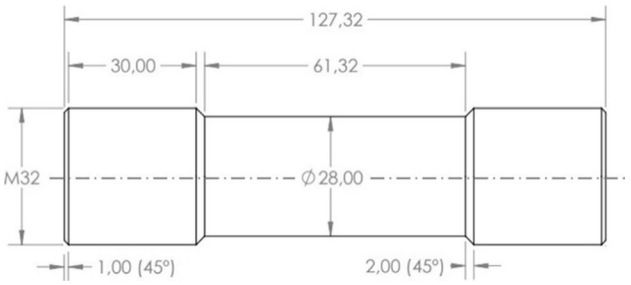

Fig. 2 Specimen final geometry

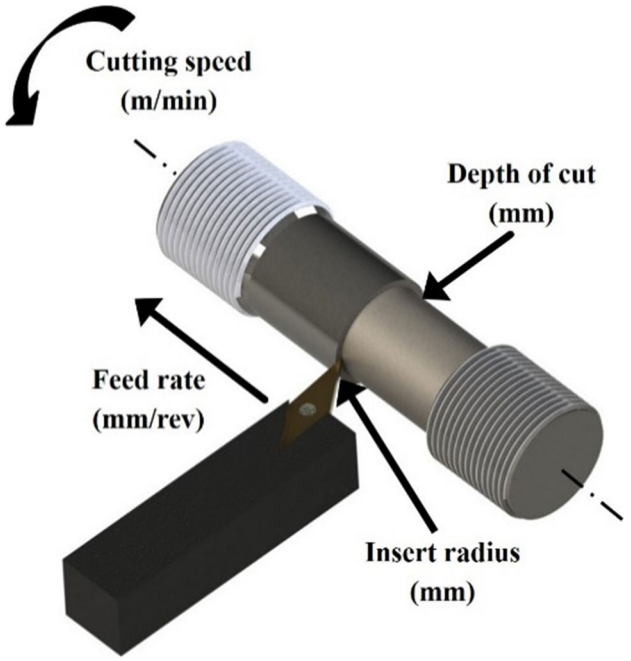

Fig. 3 Principal parameters of the turning process

To take the impact of tool radius on machining into account, two finishing inserts with two different tip radii (0.4 mm and 0.8 mm) were selected. The technical and dimensional characteristics of both inserts used together with the operating regions recommended by the insert manufacturer are shown in Table 4.

Finally, the ranges of the depths of cut and feed rates were defined between (0.05–0.25 mm) and (0.1–0.25 mm/rev), respectively. A resume of the machining parameters ranges is shown in Table 5. As can be seen, the tools will not always work within their optimum operating range, which will give new insights into the impact of these conditions on both roughness and residual longitudinal stress.

2.4 Design of experiments

A design of experiment methodology based on the response surface method was used for the scheme of the experimental campaign. The RSM is a set of mathematical and statistical techniques that allow the study of the impact of one or more input variables on the response variables of a given problem through an empirical model [22]. Due to its versatility and capacity, this methodology is used in numerous areas of knowledge, from the medical to the industrial field, for the design of experiments or the adjustment of processes. In the field of manufacturing engineering, it has been widely used to study the impact of the cutting conditions of material removal processes (turning, milling, etc.) as well as to optimize these conditions in order to reduce tool wear and to study the surface finish [23, 24].

Table 3 JATOR TAJ-42 CNC lathe technical specifications

CNC lathe Jator TAJ-42	
Machine software	Fagor 8055 T
Main speed engine power	11/15 kW
Max. spindle speed	3000 rpm
Spindle nose	DIN 55026 (A5)
Bar trough	42 mm
Automatic tool changer	12 tools
Working area (*Z*/*X*)	500/200 mm
Rapid feed (*Z*/*X*)	15/12 m/min

Among the different designs of experiments available, a CCD, also known as the Box-Wilson CCD, has been selected. This type of design consists of central points (normally between 4 and 6), which enable the correct fit of the model to be analyzed and the pure experimental error estimation. These central points are extended with axial or star points, by means of which the quadratic effects can be analyzed. Thanks to this design, the first- and second-order terms can be efficiently estimated [25].

The experimental design used for this work was done through Design Expert v13 software. The inputs of the model are 4 factors: feed rate (f_n), cutting speed (V_c), depth of cut (a_p), and insert radius (R). The first three factors are numerical variables while the last one is a categorical variable (there are few values, and only two of them are used in the proposed experimental campaign). There are also 2 responses: roughness and residual stress. Both responses are numerical continuous variables. From these input variables, 4 equations will be obtained (2 equations for each tool radius used) with which the value of the residual stress and roughness can be predicted. The ranges of input parameters of the model are shown in Table 6. The use of the CCD (central composite design) in experiments involves defining three groups of design points: two-level factor points (min. level and max. level as shown in Table 6), center points (center in Table 6), and axial points (axial min. and axial max. in Table 6). The two-level factor points and the center points define the primary design space where predictions are expected to be reliable. In contrast, the axial points are crucial for accurately

Table 4 Insert technical specifications

Insert specifications		
Insert manufacturer	Sandvik Coromant	Sandvik Coromant
Reference	DCMX 11 T3 04-WF 4325	DCMX 11 T3 08-WF 4425
Tip radius (mm)	0.4	0.8
Main cutting edge angle (°)	93	93
Recommended depth of cut (mm)	0.3–3	0.3–3
Recommended cutting speed (m/min)	345–475	305–420
Recommended feed rate (mm/rev)	0.07–0.30	0.12–0.4

Table 5 Machining parameter ranges selected for the machining process

Experimental campaign parameters	
Insert radius (mm)	0.4 and 0.8
Depth of cut (mm)	0.05–0.25
Cutting speed (m/min)	76–200
Feed rate (mm/rev)	0.1–0.25

identifying the response surface curvature and capturing the model's behavior in extreme cases. However, predictions at these axial values may be less accurate due to the lower density of points in this region and their position outside the primary design space defined by the factor and center points.

2.5 Turning process

For the machining process, a parametric numerical control program was developed to reduce programming times. During the process, several roughing passes were performed on the 35 mm bar. Thereafter, at least the 3 finishing passes were performed in each specimen employing the finishing inserts selected in Section 2.3. In order to ensure that tool wear does not affect the roughness or residual stresses obtained, the tool was changed every 2 machined specimens. The environmental conditions in the laboratory during the machining process were 25.1 °C and a relative humidity of 68%.

2.6 Residual stresses measurement

The longitudinal residual stresses derived from the machined process were measured by means of a Stresstech 3000-G3R X-ray diffractometer. The {221} gamma lattice plane was examined under a 2θ angle of 156.1°, utilizing the Kα chromium wavelength (0.2291 nm).

To obtain the values of the residual stresses, the $\sin^2\psi$ technique [26] was implemented by means of the following equation:

$$\sigma_\phi = \left(\frac{E}{1+\upsilon}\right)_{(hkl)} \left(\frac{1}{d_{\phi 0 hkl}}\right) \left(\frac{\partial d_{\varnothing\psi hkl}}{\partial \sin^2\psi}\right) \quad (1)$$

where E and ν are the elastic modulus and Poisson's ratio of the 42CrMo4 + QT steel, in the measured crystallographic plane, taken as 206 GPa and 0.296, respectively, while d is the interplanar distance of the selected diffraction plane (hkl), ψ is the tilt angle, and ϕ the angle in the same plane. Table 7 reflects the configuration of the diffractometer used for the determination of the residual stresses.

2.7 Roughness measurement

A Leica DCM3D confocal microscope was used to measure the surface roughness of the specimens. In comparison with other methods used for surface roughness assessment, the use of a confocal microscope allows a better three-dimensional description of the measured surface [27]. As one of the most commonly used, average roughness value (R_a) was selected as the reference parameter to evaluate surface roughness in this experimental campaign. R_a measurements were carried out at three different points in the central area of the specimen in accordance with the UNE-EN-ISO 21920–3 standard [28]. The cut-off filter, λ_c, was equal to 0.8 mm, and 7 repetitions were made, which conducts to the evaluation

Table 6 Input parameters and corresponding levels used for the model

Input	Type	Factor	Units	Axial min	Axial max	Design point space		
						Min. level	Center	Max. level
Feed rate	Numerical	f_n	mm/rev	0.05	0.25	0.1	0.15	0.2
Cutting speed	Numerical	V_c	m/min	76	200	107	138	169
Depth of cut	Numerical	a_p	mm	0.05	0.25	0.1	0.15	0.2
Insert radius	Categorical	R	mm	0.4	0.8	–	–	–

length of 5.60 mm. Once again, the measurement direction was longitudinal, as in the case of the residual stresses. The main configuration of the equipment can be found in Table 8.

2.8 Results evaluation

The design of experiments addressed in Section 2.4 allows not only to establish the experimental campaign, but also to analyze the results of these experiments thanks to its built-in statistical tools. Figure 4 summarizes the RSM developed in this work, highlighting the relation between the design of experiments explained in Section 2.4 and the final predictive equations. Four predictive equations were obtained (2 for each response and insertion radius), which allow for estimating both residual stress and roughness values as a function of the 4 input factors.

3 Experimental results

This section presents the results of the experimental campaign designed in Section 2 (see Table 16 in the Appendix). Furthermore, a critical and pivotal analysis of the results is carried out in which the discrepancies obtained in some of the samples show a different roughness or residual stress, despite being machined under the same cutting conditions, are discussed.

3.1 Critical analysis of results

A closer inspection of the results reveals discrepancies in the experimental values obtained. This is the case for specimens 45 and 46, which, despite being machined in the same scenario, show significant differences in terms of roughness and residual stresses as shown in Table 16 in the Appendix. Figure 5 establishes a comparison between the surface obtained for specimen 45 (a) and for specimen 46 (b), showing the presence of large grooves along the length of specimen 45, which may have induced the high roughness measured in this specimen. Figure 5c, d shows the R_a roughness numerical values measured in the longitudinal direction of specimens 44 and 45, respectively.

Scatter of the results is always expected when an experimental campaign is performed. Nevertheless, it is always necessary to identify the results that are out of the scope, which must be treated as outliers. These outliers can be produced by numerous causes, such as equipment failure, human errors, or measurement errors [29]. Identifying those specimens that could be classified as outliers is of vital importance for the correct modeling of the subsequent response surface. For this purpose, powerful statistical tools are required to determine whether such experimental outputs can be treated as outliers or they cannot. Including them in the model without carrying out this prior

Table 7 Experimental parameters for residual stress measurements

Stresstech 3000-G3R X-ray diffractometer setup	
Maximum voltaje (kV)	30
Exposure time (s)	20
Tilt Ψ (°)	5 points (−45° to +45°)
Noise reduction	Parabolic
Filter of Kα radiation	Vanadium
Maximun intensity (mA)	6.7
Collimator diameter (mm)	2 (short type)
Goniometric rotation (measurement direction) Ø (°)	0
Peak adjustment	Pseudo-Voigt

Table 8 Experimental parameters for roughness measurements

Leica DCM3 confocal microscope setup	
Used standard	ISO-21920–3
Objective magnification	10x
Measured parameter	R_a
Selected cutt-off (λ_c) (mm)	0.8
Evaluation length (mm)	5.60
Evaluation width (mm)	0.95
Evaluation area (mm^2)	5.32

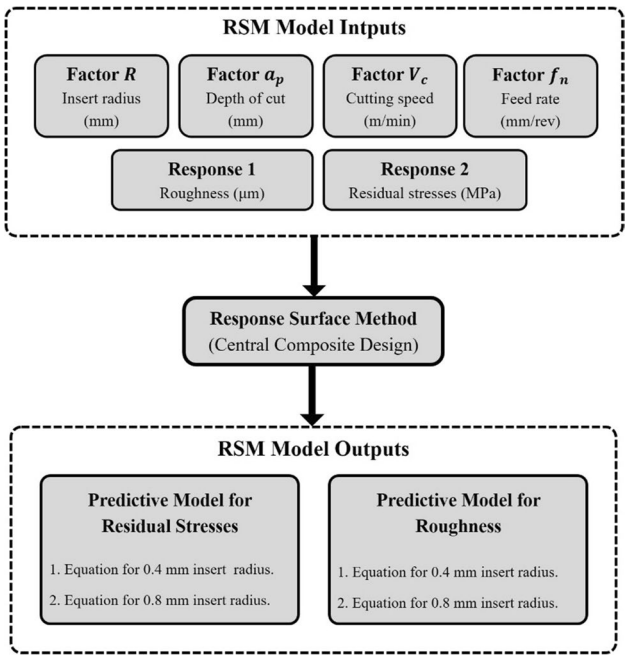

Fig. 4 Outline of the response surface method designed with inputs and outputs

analysis may result in an incorrect fitting of the model. The statistical tools used to identify those samples are described below.

In order to identify and analyze these outliers, the methodology shown in Fig. 6 was implemented. Once the residual stress and roughness were measured, a preliminary fit of the model was done, which was then analyzed by means of the statistical diagnostic tools which are explained as follows.

The first statistical tool allows the user to determine whether the externally studentized residuals are normally distributed. To do this, the percentiles of the theoretical normal distribution are plotted against the percentiles of the experimental residuals. If the externally studied residuals follow a normal distribution, the plot of the theoretical percentiles of the normal distribution overlaps with the plot of the observed percentiles of the sample. The second tool presents the externally studied residuals against the expected residuals as the output parameters (in this work, roughness and residual stresses) increase, allowing the hypothesis of homogeneity of variances to be tested independently of the value of the response [30]. Similar to the previous one, the third statistical tool consists of plotting the externally studentized residuals against the residuals obtained in each of the samples of the experiment, thus allowing to identify hidden variables that may have influenced the response. The externally studied residual, also known as the outlier *t*-value or RStudent, is calculated by excluding one series at a time from the analysis and predicting the response based on the remaining series. This involves estimating the response without the contribution of each specific series. The resulting *t*-value represents the difference, in terms of standard deviations, between the predicted value and the actual response. Essentially, this assessment determines whether the excluded run fits the model using coefficients derived from the remaining runs [30]. In other words, it tests whether the omitted run is in harmony with the overall pattern of data for the specified model. Finally, the Box-Cox Plot is used

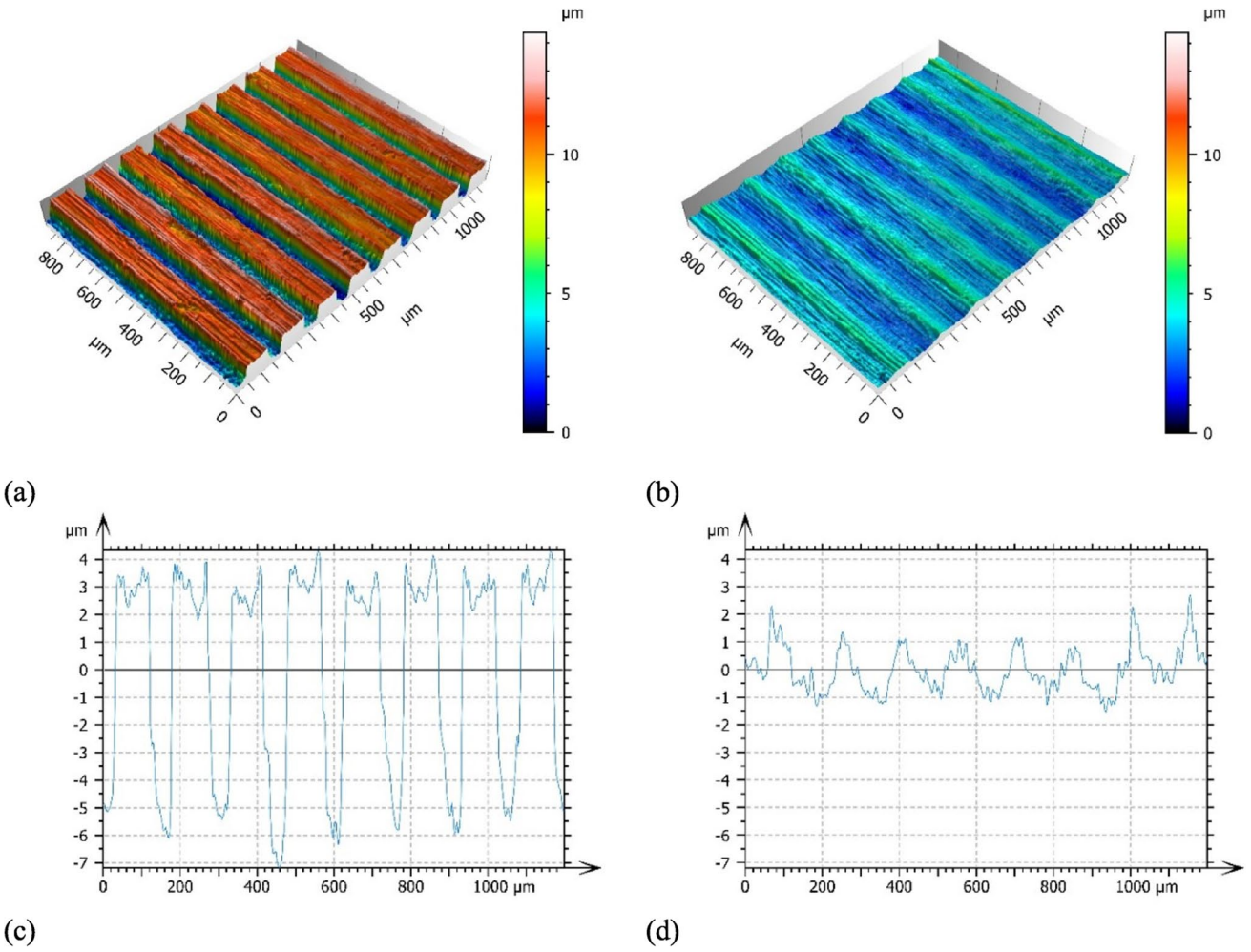

Fig. 5 Surface defects generated during the turning process of two specimens machined in the same scenario: **a** 3D representation of the surface of specimen 45; **b** 3D representation of the surface of specimen 46; **c** Measured R_a values along the surface for 45 specimens; and **d** measured R_a values along the surface for 45 specimens

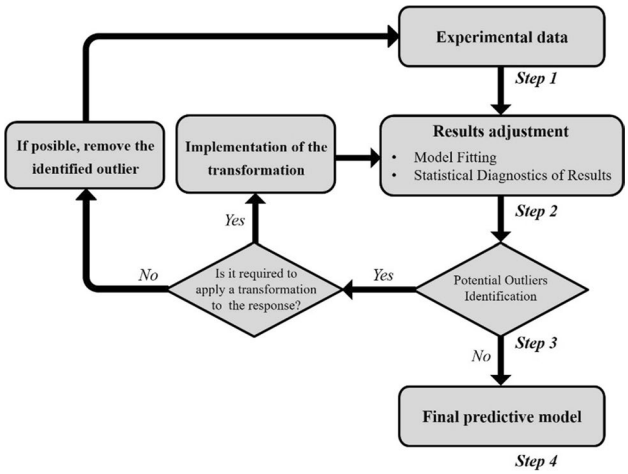

Fig. 6 Proposed methodology to assess the experimental data in order to identify the suitable outliers

to determine whether any transformation of the response is necessary [31]. The latter tool shows the recommended transformation based on the actual lambda value applied to the response and the lower point of the curve generated by the natural logarithm of the sum of the squares of the residuals, been the difference between both values directly related to the required transformation. The implementation of the methodology described above can be seen in Section 4.

If a potential outlier is observed by using any of the presented statistical tools, the first step is to check whether any transformation of the response is necessary before considering the sample as an outlier. Regardless of the followed path, a readjustment of the previous model is therefore essential. This iterative process is applied until the outliers identified are eliminated, pursuing a compromise between having no outliers and not biasing the model. Tables 9. and 10 show, respectively, the outliers identified for each response.

4 Proposed predictive models

The following section presents the models obtained for both residual stress and roughness. Section 4.1 presents the complete statistical summary of the model according to the methodology explained above, the correlations between roughness and machining parameters, and, finally, two predictive equations for the surface roughness estimation model, one for the 0.4 mm insert radius and one for the 0.8 mm insert radius. In Section 4.2, a similar approach is adopted for the residual stress estimation model.

4.1 Predictive model for roughness

The impact of the different machining factors on the surface roughness is graphically shown in Fig. 7. On the one hand, among the numerical variables, the variable with the greatest impact on the surface roughness is the feed rate with a correlation coefficient of 0.737, while the cutting speed and depth have a much lesser influence on the surface roughness of the samples, with a correlation coefficient of − 0.053 and − 0.191 respectively. On the other hand, an analysis of the categorical variable shows that as the tool radius increases, roughness decreases.

The aforementioned correlation coefficients are obtained using the Pearson correlation coefficient (r), which is mathematically defined as follows:

$$r = \frac{\sum_{i=1}^{n}(x_i - \bar{x})(y_i - \bar{y})}{\sqrt{\sum_{i=1}^{n}(x_i - \bar{x})^2 \sum_{i=1}^{n}(y_i - \bar{y})^2}} \quad (2)$$

where x_i and y_i are the individual values of the variables x and y, $\bar{x}$, and $\bar{y}$ are the means of the variables x and y, respectively, and finally, n represents the number of data pairs. The Pearson correlation coefficient can take values between − 1 and 1, where a value of 1 indicates a perfect positive correlation, − 1 indicates a perfect negative correlation, and 0 indicates no correlation between the two variables under study.

Figure 8 presents the diagnostic plots after iteratively applying the statistical methodology explained in the previous section for the detection of possible outliers where a natural logarithmic transformation of the roughness was required. Figure 8a shows the correct fit of the externally studentized residuals to a normal distribution. Figure 8b, c show how the externally studentized residuals conform to the principle of homogeneity in variances independently of the increase in response (b) or the run number (c). Finally, Fig. 8d shows the result of the Box-Cox plot for the evaluation of the possible transformations required in the response after applying the recommended logarithmic transformation. It shows that no transformation is necessary.

Model coefficients are shown in Table 11. The significance level used to consider a term significant or not is 0.05. Thus, those terms whose associated p-value is below the threshold of 0.05 are considered significant. Those terms included in the model with an associated p-value greater than 0.05 are necessary to maintain the hierarchy of the model (in this case, $V_c \bullet R$, and $V_c{}^2$); hence, they are retained. On the other hand, the model shows a non-significant lack of fit with an associated p-value of 0.1547. Table 12 shows a difference of less than 0.2 between the predicted R^2 and the adjusted R^2. Furthermore, the value of Adeq. precision (which measures the signal to noise ratio) of 34.5 is much higher than the minimum value of 4.0 estimated for this

Table 9. Identified outliers for the roughness model

Run	Factor R: insert radius (mm)	Factor a_p: depth of cut (mm)	Factor V_c: cutting speed (m/min)	Factor f_n: feed rate (mm/rev)	Response 1: Ra roughness (μm)	Response 2: residual stresses (MPa)
14	0.4	0.15	138	0.05	0.657	-513.3
36	0.8	0.05	138	0.15	1.069	496.4
45	0.8	0.15	76	0.15	3.235	133.0
61	0.8	0.2	107	0.2	1.259	669.6
65	0.8	0.2	169	0.1	0.54	24.8

Table 10 Identified outliers for the residual stresses model

Run	Factor R: insert radius (mm)	Factor a_p : depth of cut(mm)	Factor V_c : cutting speed (m/min)	Factor f_n: feed rate (mm/rev)	Response 1: Ra roughness (μm)	Response 2: residual stresses (MPa)
10	0.4	0.1	169	0.1	0.561	122.3
12	0.4	0.15	76	0.15	0.806	102.5
15	0.4	0.15	138	0.15	0.796	141.3
27	0.4	0.2	107	0.2	1.002	519.7
38	0.8	0.1	107	0.1	0.551	-253.1
52	0.8	0.15	138	0.15	0.41	545.9
53	0.8	0.15	138	0.15	0.475	538.7
66	0.8	0.2	169	0.1	0.372	374.9
67	0.8	0.25	138	0.15	0.367	67.2

parameter, so that the model is able to make accurate predictions within the design space.

Figure 9 shows the roughness response surfaces for the 0.4 mm tool radius insert (Fig. 9a) and for the 0.8 mm radius insert (Fig. 9b), derived for fixed depth of cut of 0.15 mm, which corresponds to half of the range of values that the depth variable takes in the experimental campaign. Taking into account that the depth of cut is the variable that has a lower impact on the results, the response surfaces obtained for other depths inside the workspace would be similar to the ones represented in Fig. 9. A more detailed analysis of both response surfaces reveals a completely opposite behavior in terms of cutting speed. On the one hand, for those specimens machined with a 0.4 mm insert, it can be observed that at the same feed rate, the roughness reaches its maximum for a cutting speed of around 126 m/min, decreasing for cutting speeds higher or lower than this value. On the other hand, for those samples machined with a 0.8 mm insert, it can be observed that at the same feed rate, the estimated roughness reaches its minimum when the cutting speed is around 150 m/min, increasing as the cutting speed moves away from this value. Moreover, the highest roughness values are expected for those specimens machined with the 0.4 mm inserts under high feed rates. Figures 10 and 11 establish a comparison between the experimental results and the values obtained on the basis of the predictive models developed previously, showing the correct adequacy of these for the prediction of roughness.

Finally, the equations of the predictive model are introduced to estimate the roughness value as a function of the turning process parameters:

For insert radius $(R) = 0.4$

$$\begin{aligned}\ln\left(R_a + 0.5\right) = {} & -0.936195 + 4.79502\, f_n + 0.008349\, V_c \\ & - 0.287258\, a_p - 0.016195\, (V_c \cdot a_p) - 0.000023\, (V_c)^2 \\ & + 6.26819\, (a_p)^2\end{aligned} \tag{3}$$

For Insert radius $(R) = 0.8$

$$\begin{aligned}\ln\left(R_a + 0.5\right) = {} & 0.407991 + 2.34984\, f_n - 0.00756\, V_c \\ & - 1.09785\, a_p - 0.016195\, (V_c \cdot a_p) \\ & - 0.000034\, (V_c)^2 + 6.26819\, (a_p)^2\end{aligned} \tag{4}$$

where R_a corresponds to the roughness parameter expressed in μm, f_n is the feed rate in mm/rev, V_c is the cutting speed expressed in m/min, and a_p is the depth of cut in mm.

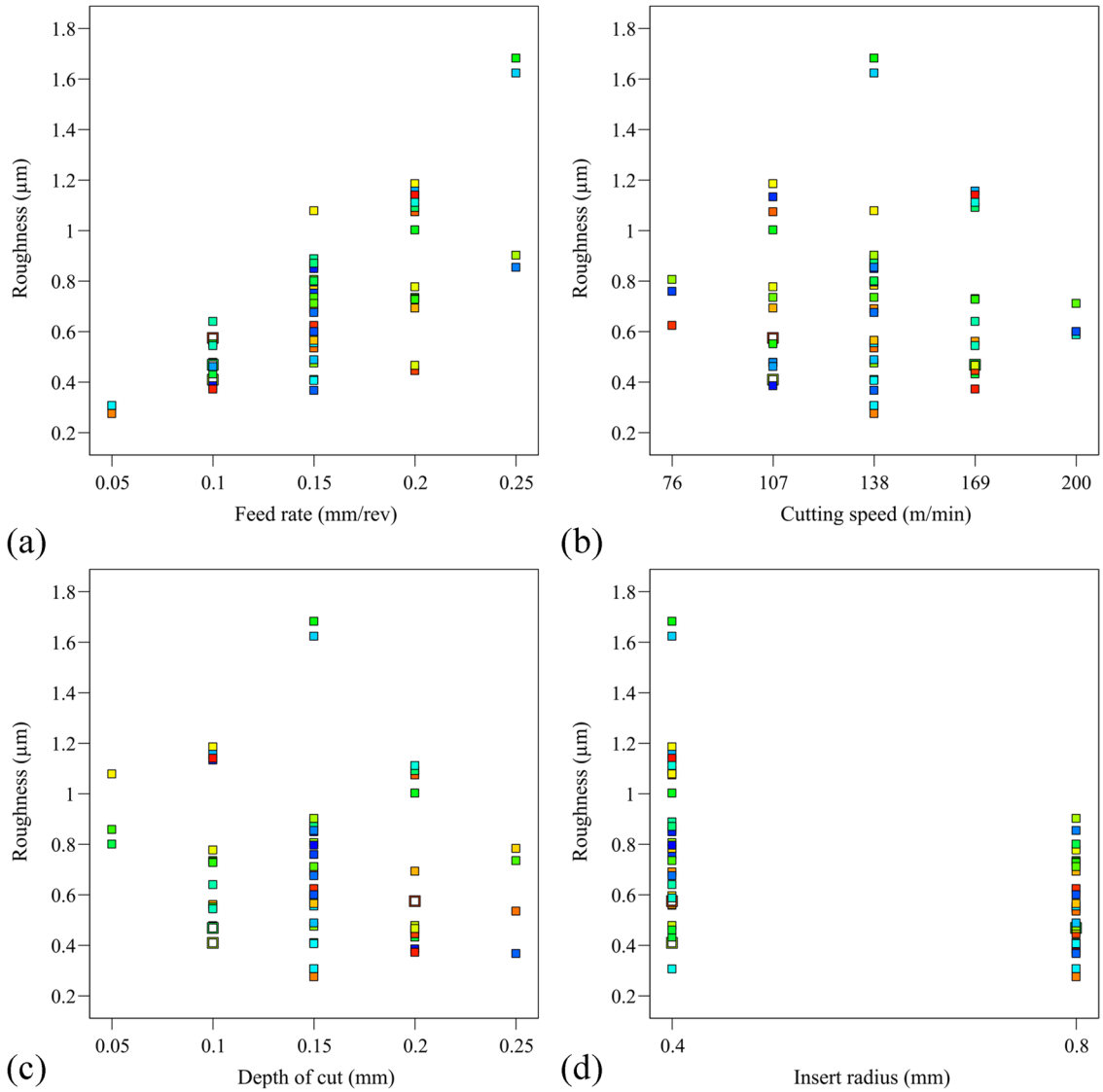

Fig. 7 Correlation between factors and roughness: **a** feed rate vs roughness; **b** cutting speed vs roughness; **c** depth of cut vs roughness; and **d** radius vs roughness

4.2 Predictive model for residual stresses

The analysis performed for residual stresses is analogous to that performed for roughness. Thus, Fig. 12 introduces the correlations between the input variables and the residual stress measured after the experimental campaign. As in the case of roughness, the variable that seems to have the greatest impact on the residual stresses generated on the surface of the feed rate, with a Pearson correlation coefficient factor (obtained by means of Eq. (2)) of 0.838, while the correlations coefficients for cutting speed and depth are 0.062 and − 0.028, respectively. Moreover, a change in tool radius does not seem to have a significant influence on the longitudinal residual stresses.

The diagnostic plots show a correct normal distribution of the externally studentized residuals (Fig. 13a) as well as the homogeneity of the observed variances independent of residual stress values and sample number (Fig. 13b, c) once the recommended transformation has been applied. The transformation used to adjust the residual stresses data is a power law one, with lambda equal to 1.85 and a constant k equal to 627.645 according to the Box-Cox plot recommendations.

The coefficients of the different terms of the model are shown in Table 13. The lack of fit shows an associated p-value of 0.5996, while the model has an associated F-value of 58.63, which indicates the significance of the model. Table 14 shows the coefficients of variation associated with the model, where the difference between the

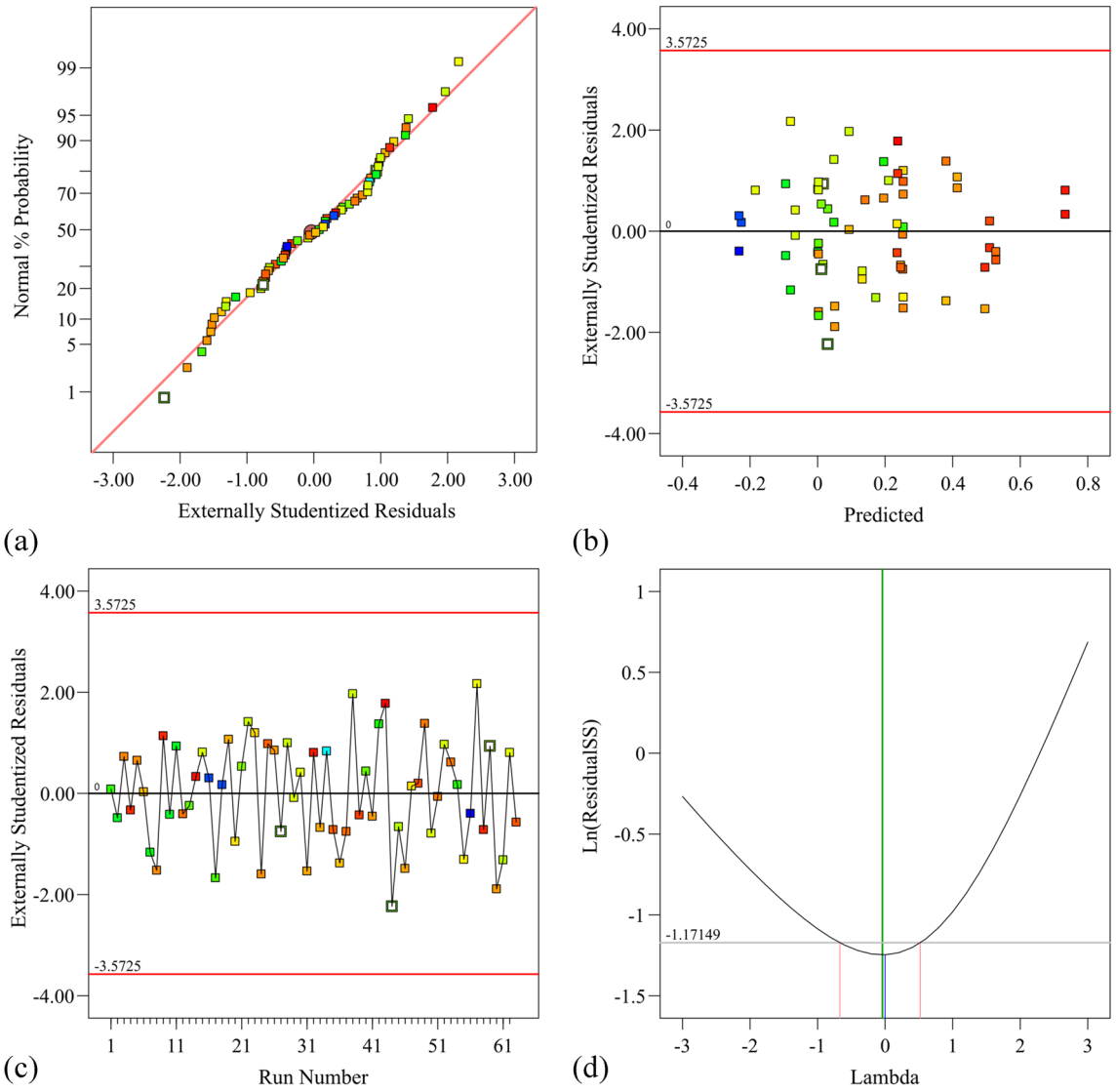

Fig. 8 Diagnostic plots for Roughness: **a** externally studentized residuals vs normal % probability; **b** externally studentized residuals vs predicted; **c** externally studentized residuals vs run number; and **d** Box-Cox plot for power transforms

predicted R^2(0.9162) and the adjusted R^2 value (0.8976) is less than 0.2, thus showing a reasonable agreement.

Figure 14 shows the residual stress response surfaces for the specimens machined with the 0.4 mm tip radius insert (Fig. 14a) and the 0.8 mm insert (Fig. 14b). As regards the response in residual stress values, the depth is again the lowest weight value for both tool radius, so to obtain the response surface its value is set to 0.15 mm. A more detailed analysis of both response surfaces shows the existence of significant differences between them with respect to the influence of the cutting speed. On the one hand, the response surface for the specimens machined with the 0.4 mm tool shows how the variation of the cutting speed has hardly any influence for low feed rates, while for higher feed rates some impact can be seen can be seen. By setting a feed rate of 0.2 mm/rev, the tensile residual stresses reach their maximum value, while they decrease for higher cutting speeds. On the other hand, the response surface for the specimens machined with the 0.8 mm tool shows how the variation of the cutting speed has hardly any influence on high feed rates, whereas it does for low feed rates. Thus, by setting the feed rate to 0.1 mm/rev, it can be seen that for low cutting speeds compressive residual stresses are obtained, while for higher cutting speeds the residual stresses are positive. In both surfaces, it can be seen that an increase in the feed rate leads to higher residual stresses. Figure 15 shows a correct fit of the phenomenological models obtained for both the 0.4 and 0.8 radii, with all results falling in the central area of the graph.

Table 11 Analysis of variance for roughness predictive model

Source	Sum of squares	df	Mean square	*F*-value	*p*-value
Model	3.04	11	0.2761	67.17	< 0.0001
f_n– feed rate	1.83	1	1.83	445.13	< 0.0001
V_c– cutting speed	0.0177	1	0.0177	4.30	0.0431
a_p– depth of cut	0.1556	1	0.1556	37.86	< 0.0001
R– insert radius	0.6111	1	0.6111	148.68	< 0.0001
$f_n \bullet R$	0.2143	1	0.2143	52.13	< 0.0001
$V_c \bullet a_p$	0.0187	1	0.0187	4.55	0.0377
$V_c \bullet R$	0.0002	1	0.0002	0.0522	0.8201
$a_p \bullet R$	0.0233	1	0.0233	5.67	0.0210
${V_c}^2$	0.0021	1	0.0021	0.5029	0.4815
${a_p}^2$	0.0198	1	0.0198	4.81	0.0328
${V_c}^2 \bullet R$	0.0642	1	0.0642	15.61	0.0002
Residual	0.2096	51	0.0041		
Lack of fit	0.0941	18	0.0052	1.49	0.1547
Pure error	0.1155	33	0.0035		
Cor total	3.25	62			

Table 12 Regression parameters for roughness model

Std. dev	0.0641	R^2	0.9354
Mean	0.1580	AdjustedR^2	0.9215
C.V. %	40.56	PredictedR^2	0.8966
		Adeq.precision	34.5101

Finally, the two predictive equations obtained for the determination of the longitudinal residual stresses are presented.

For insert radius (R)= 0.4 mm

$$\left(\sigma_{RSL}+627.65\right)^{1.85} = -780996 + 9569110 f_n + 4687.59618 V_c + 315040 a_p - 21069.41(f_n \cdot V_c) - 14143.15(V_c \cdot a_p) - 13474900\left(f_n\right)^2 + 5651830\left(a_p\right)^2 \quad (5)$$

For Insert radius (R) = 0.8 mm

$$\left(\sigma_{RSL}+627.65\right)^{1.85} = 856760 + 6203690 f_n + 5989.03239 V_c + 315040 a_p - 21069.41(f_n \cdot V_c) - 14143.15(V_c \cdot a_p) - 981032(f_n)^2 + 5651830\left(a_p\right)^2 \quad (6)$$

where σ_{RSL} corresponds to the longitudinal residual stress expressed in MPa, f_n is the feed rate in mm/rev, V_c is the cutting speed expressed in m/min and a_p is the depth of cut in mm. A more exhaustive comparison between the experimental results and the proposed models can be seen in Fig. 16, showing the correct fit of the models for each insert radius.

5 Discussion

In this section, a comparative analysis is conducted between the results obtained from the models proposed in this study and those proposed in the literature for the same purpose.

On the one hand, the most widespread model to predict the estimated value of surface roughness, R_a, as a function of cutting parameters [15] is as follows:

$$R_a = \frac{1000\, {f_n}^2}{32\, R} \quad (7)$$

where R_a corresponds to the average roughness parameter expressed in µm, while f_n and R refer to the feed rate expressed in mm/rev and the tool tip radius in mm,

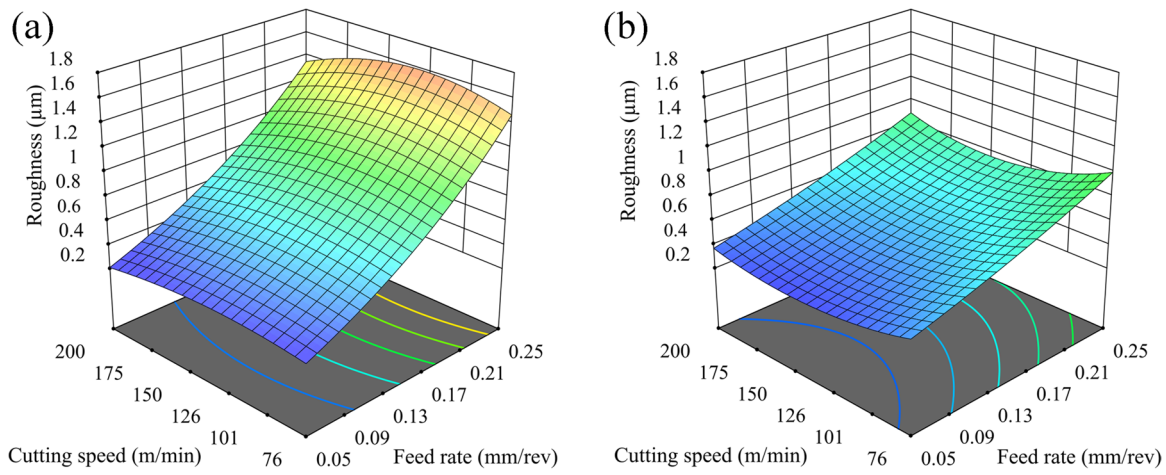

Fig. 9 Response surfaces for roughness: **a** response surface for 0.4 mm insert radius and **b** response surface for 0.8 mm insert radius

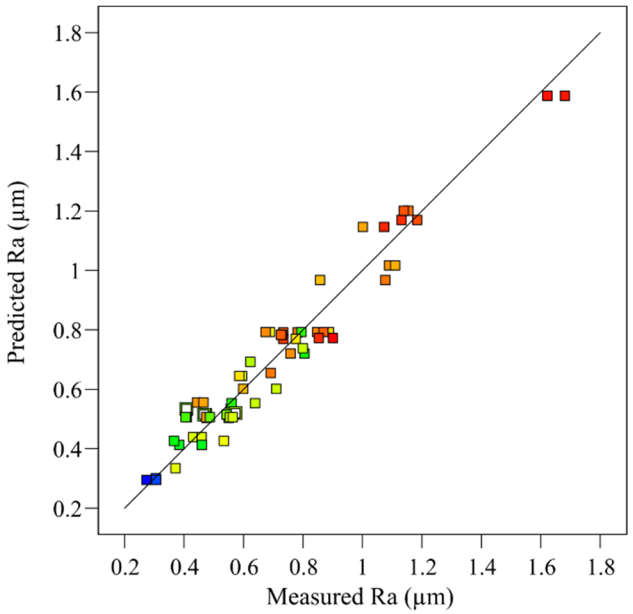

Fig. 10 Predicted vs measured roughness parameters

respectively. A graphical comparison based on the results found before has been made in Fig. 17, showing again the good results obtained with the roughness model for both the 0.4 mm (a) and 0.8 mm (b) tool insert radius. Table 17 in the Appendix compares the predictions made by the model proposed in this paper with the ones derived from Eq. (7). The results shown in Table 17 in the Appendix, reveal that Eq. (7) gives rise to significantly higher relative errors compared to the models proposed in this study, which highlights the effectiveness of the model developed in the prediction of the surface roughness parameter, R_a, under the selected machining conditions. It is important to mention that Eq. (7) is expected to be valid for the finishing cutting conditions recommended by the manufacturer. The deviations in R_a observed between our experimental results and Eq. (7) are attributed to the use of cutting conditions outside this recommended range. Therefore, it is not our intention to suggest that Eq. (7) is invalid in other scenarios. We have only demonstrated that, within the space of cutting parameters tested, the proposed models yield better predictions than Eq. (7).

On the other hand, the models obtained in this study to estimate the residual stresses have been compared with those proposed in the research carried out by Capello [9], which is one of the most cited in the literature. He established that the residual stresses can be obtained by the following:

$$\sigma_{RSL} = \sigma_{rm}(HRb) + \sigma_{rp}\left(f_n, R\right) = 1000[h_1 HRb + \log\left(f_n^{\,h_2} R^{h_3}\right)] \tag{8}$$

where *HRb* corresponds to the general Rockwell B hardness value of the steel under study obtained by Capello, while f_n and R refer to the feed rate expressed in mm/rev and the tool tip radius in mm respectively. Coefficients h_1, h_2, and h_3 are the regression parameters for the 42CrMo4 steel, which can be seen in Table 15. The reader should note that there are some discrepancies between the values of the mechanical properties measured by Capello (in terms of ultimate strength (R_m) and *HRb*) in his work and those proposed here based on measurements made by the authors for 42CrMo4 + QT steel in previous works [21]. However, since hardness is one of the most critical parameters in Capello's predictive equation and in order not to bias the results, the comparison here has been made using the hardness value

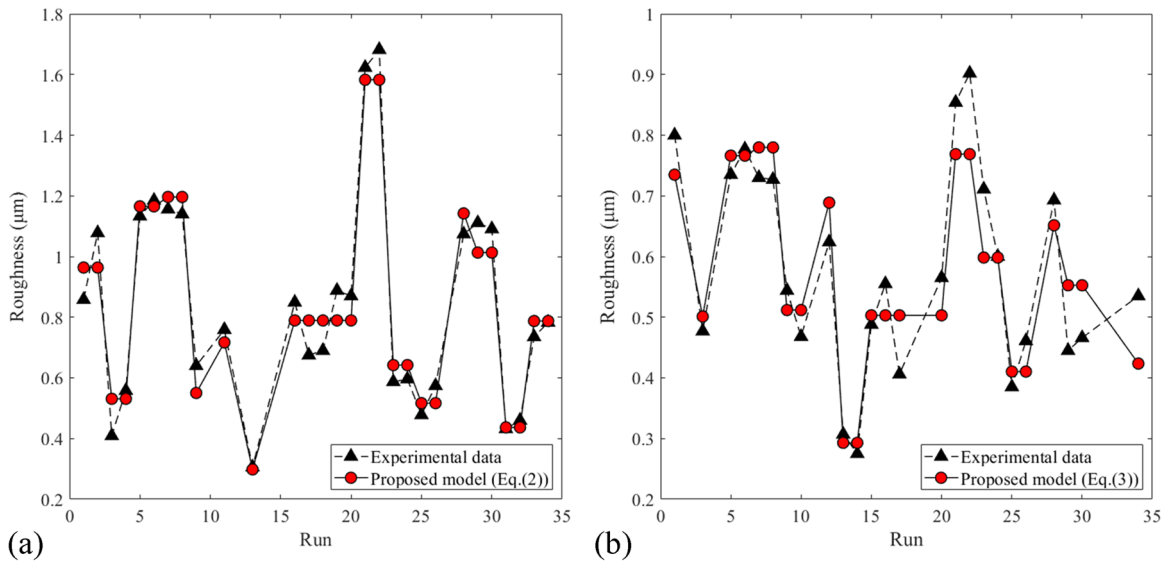

Fig. 11 Comparison of experimentally measured and predicted roughness according to the model proposed by the authors: **a** for 0.4 mm insert radius and **b** For 0.8 mm insert radius

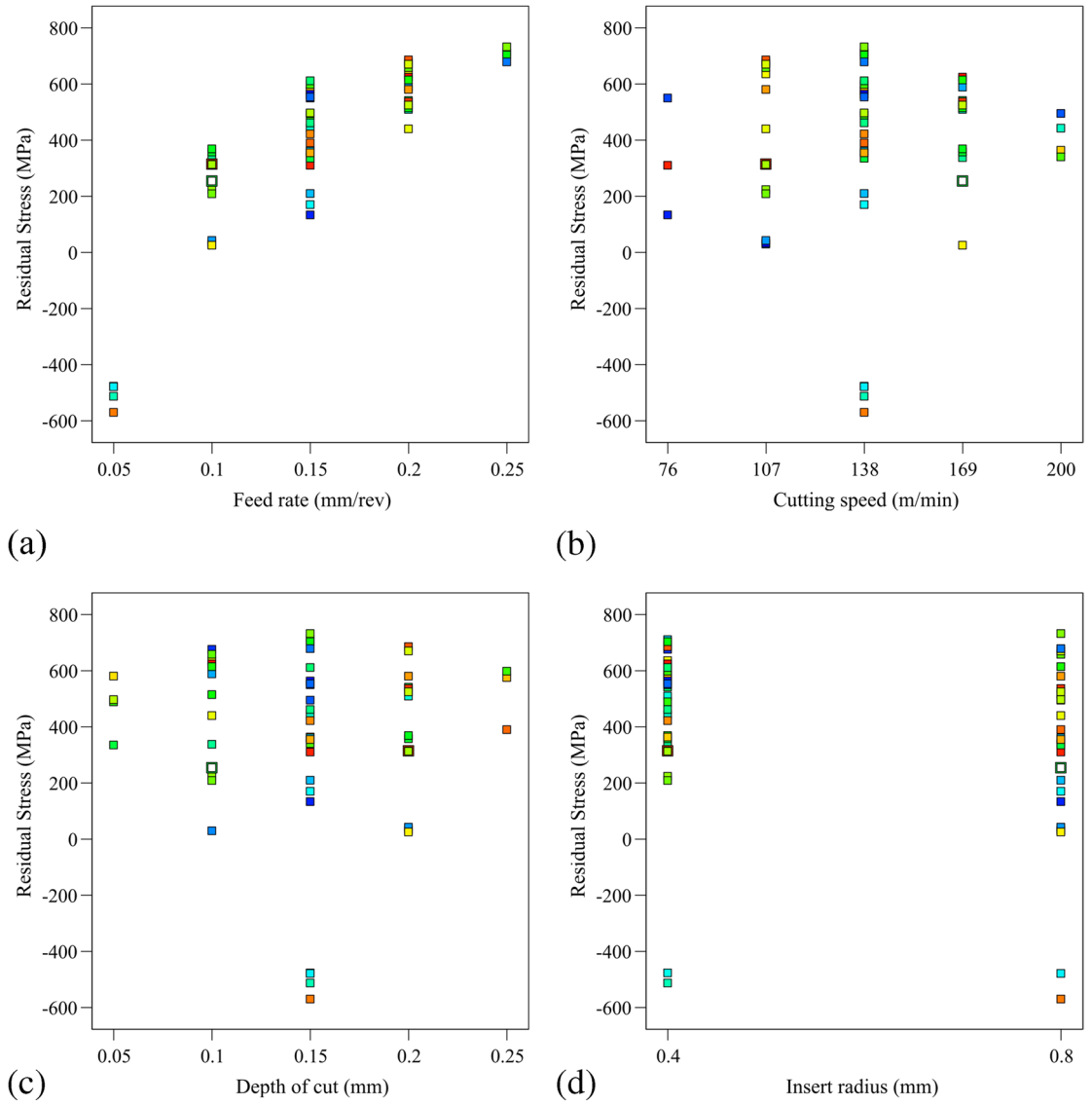

Fig. 12 Correlation between factors and residual stresses: **a** feed rate vs residual stress; **b** cutting speed vs residual stress; **c** depth of cut vs residual stress; and **d** radius vs residual stress

proposed in his original paper. This comparison of results is also shown graphically in Fig. 18, where Fig. 18a is devoted to the 0.4 mm insert radius values and Fig. 18b to those specimens machined with the 0.8 mm insert radius tool. In both cases, it can be seen how the model proposed in Capello's work fails for residual stresses close to zero or negative, while for higher values, the models tend to predict similar behavior. Analogously to what was previously proposed for the study of roughness, Table 18 in the Appendix shows the comparison of the relative percentage errors obtained in the prediction of residual stress with the model proposed here compared to those obtained with the model proposed by Capello [9], demonstrating the improvement achieved in this case. Once again, it is important to remark that the deviation between the experimental results obtained in this work and the predictions obtained by Capello's model can be caused by the values used to machining the samples, which, in some cases, are out of the scope of the Capello's work, which supposes an extrapolation of his model.

A detailed analysis of the two equations proposed in the literature underlines that among all the variables of the turning process that can affect both roughness and residual stresses, feed rate, and tool radius are the most critical parameters, being these results clearly aligned with those obtained in this experimental campaign.

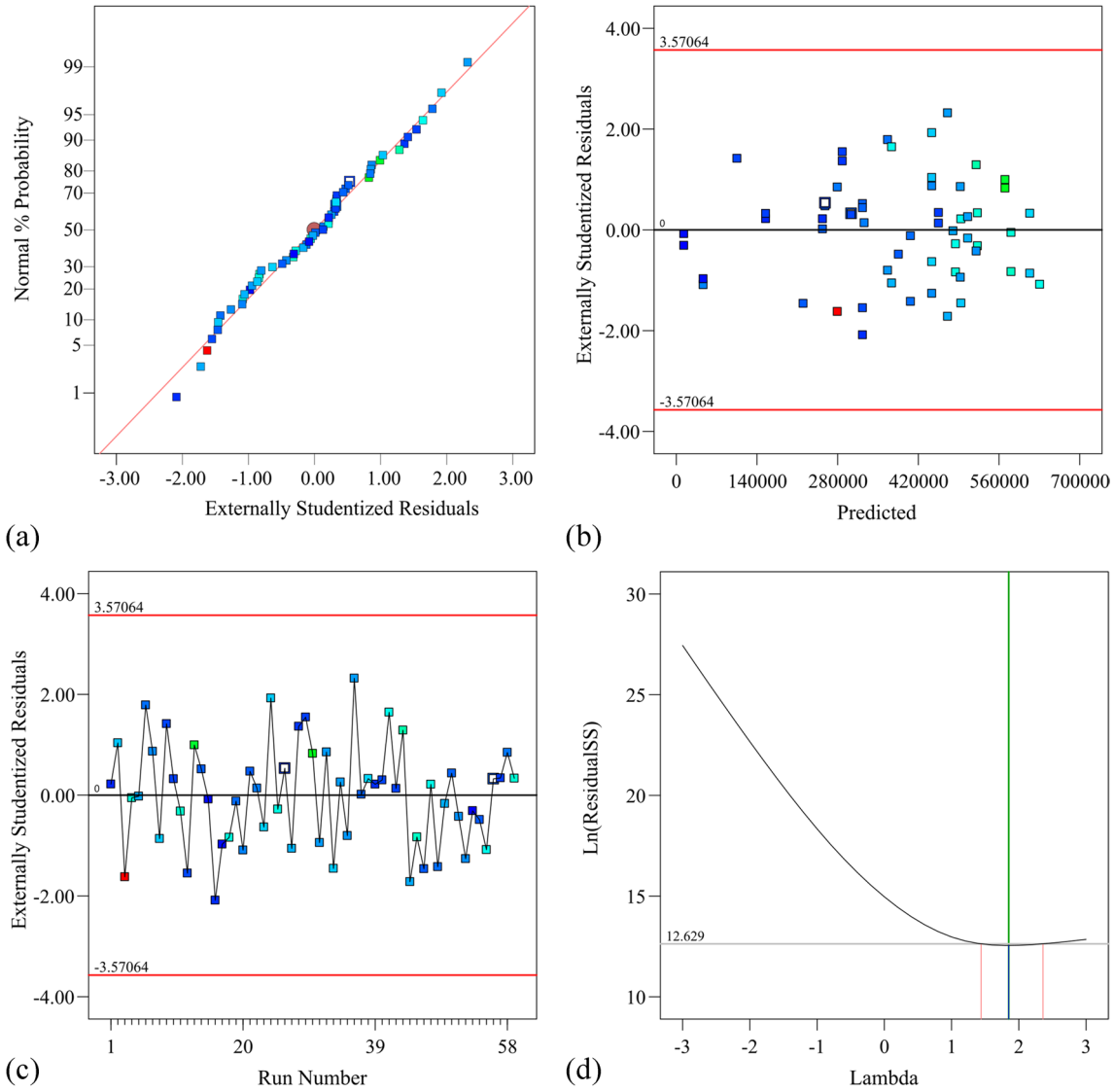

Fig. 13 Diagnostic plots for residual stresses: **a** externally studentized residuals vs normal % probability; **b** externally studentized residuals vs predicted; **c** externally studentized residuals vs run number; and **d** Box-Cox plot for power transforms

6 Conclusions

In this work, four models have been developed to estimate surface roughness and longitudinal residual stresses based on the turning conditions for 42CrMo4 + QT steel. It is important to highlight that, while these models can be crucial for machining parts or fatigue characterization specimens of this material, they are only valid within the range of cutting parameters defined in this study and for the selected material. Therefore, any extrapolation beyond these ranges is not guaranteed.

To obtain these models, a design of experiments was carried out using the central composite design method. Based on this design, 68 specimens were machined under 30 different machining scenarios in order to have sufficient information on the impact of the turning process on the surface integrity of the specimens. Subsequently, a statistical methodology was applied to identify potential outliers, which were removed from the model, thus eliminating their impact and improving the model fit. This elimination may be due to various factors such as non-uniform chips that occur during the turning process or unexpected phenomena that could

Table 13 Analysis of variance for residual stresses predictive model

Source	Sum of squares	df	Mean square	*F*-value	*p*-value
Model	1.390E+12	11	1.263E+11	58.63	<0.0001
f_n– feed rate	1.174E+12	1	1.174E+12	544.86	<0.0001
V_c– cutting speed	1.598E+08	1	1.598E+08	0.0741	0.7866
a_p– depth of cut	4.741E+08	1	4.741E+08	0.2200	0.6412
R– insert radius	1.273E+11	1	1.273E+11	59.09	<0.0001
$f_n \cdot V_c$	2.931E+10	1	2.931E+10	13.60	0.0006
$f_n \cdot Ir$	5.443E+09	1	5.443E+09	2.53	0.1187
$V_c \cdot a_p$	1.317E+10	1	1.317E+10	6.11	0.0171
$V_c \cdot Ir$	2.218E+10	1	2.218E+10	10.29	0.0024
f_n^2	2.777E+10	1	2.777E+10	12.89	0.0008
a_p^2	1.537E+10	1	1.537E+10	7.13	0.0104
$f_n^2 \cdot R$	2.307E+10	1	2.307E+10	10.71	0.0020
Residual	1.013E+11	47	2.155E+09		
Lack of fit	3.589E+10	18	1.994E+09	0.8842	0.5996
Pure error	6.540E+10	29	2.255E+09		
Cor total	1.491E+12	58			

affect the response. Further exploration and examination are required to identify and mitigate these potential influences effectively. Due to the implementation of the insert tip radius as a categorical variable in the analysis, four final equations were obtained, two dedicated to the prediction of the roughness evaluated in terms of the R_a parameter divided for each categorical factor (here insert radius, 0.4 mm, and 0.8 mm), and as the same mentioned factors, two for the evaluation of the residual stress were obtained.

Finally, a comparison was made between two of the most widely used equations in the literature to predict roughness and longitudinal residual stress, showing the advantages of the model designed here to predict both parameters under the proposed machining scenarios.

Table 14 Regression parameters for the residual stress model

Std. dev	46,422.78	R^2	0.9321
Mean	3.828E+05	AdjustedR^2	0.9162
C.V. %	12.13	PredictedR^2	0.8976
		Adeq precision	29.4998

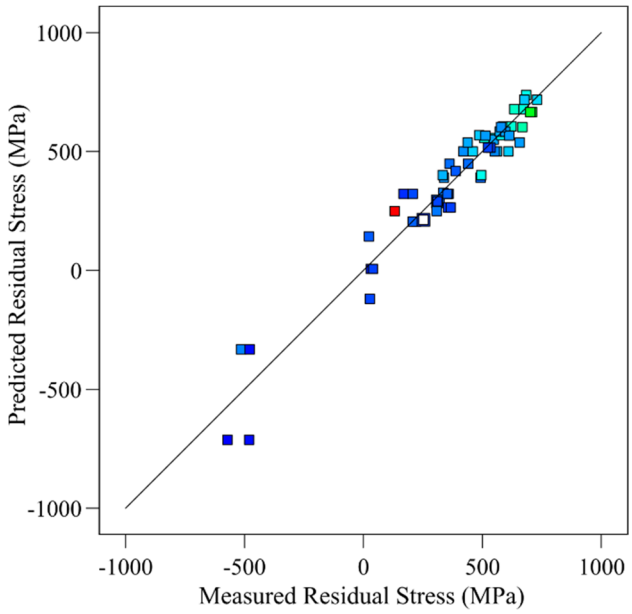

Fig. 15 Predicted vs measured residual stresses

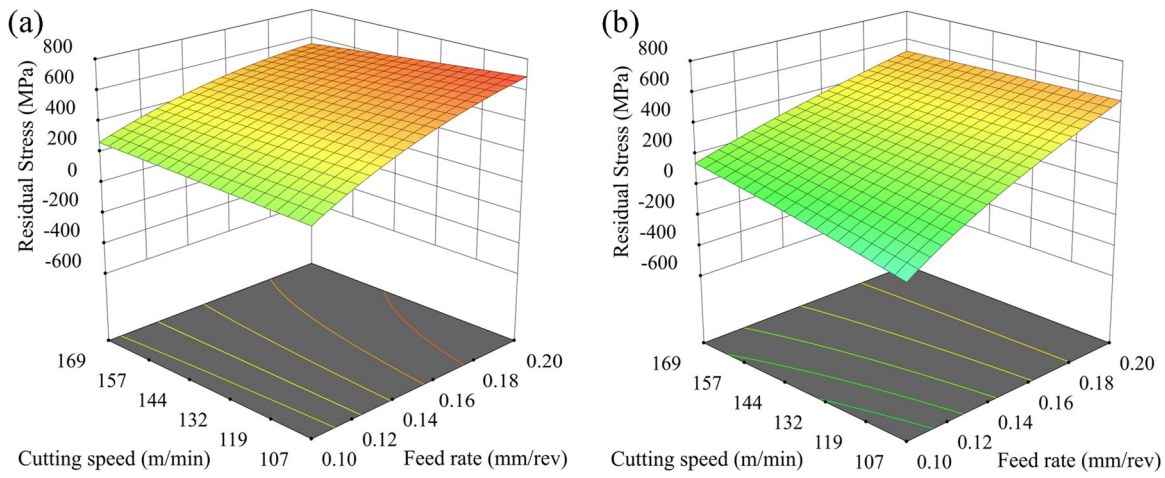

Fig. 14 Response surfaces for residual stresses: **a** response surface for 0.4 mm insert radius and **b** response surface for 0.8 mm insert radius

Appendix

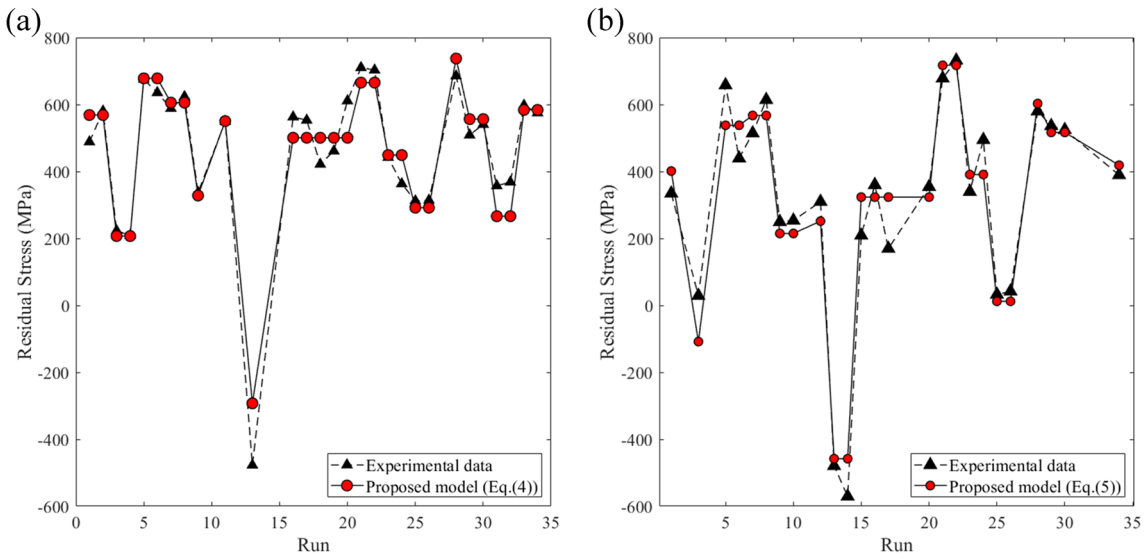

Fig. 16 Comparison of experimentally measured and predicted longitudinal residual stress according to the model proposed by the authors: **a** for 0.4 mm insert radius and **b** for 0.8 mm insert radius

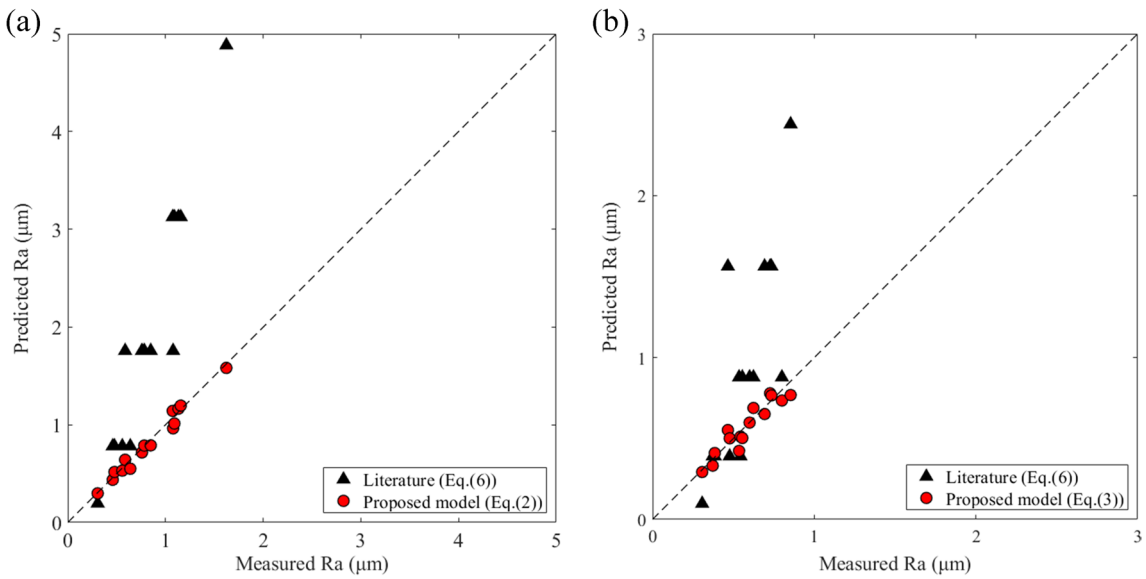

Fig. 17 Comparison of roughness estimated by the model proposed in this paper and the most used proposal in the literature (Eq. (6)): **a** for 0.4 mm insert radius and **b** for 0.8 mm insert radius

Table 15 Estimated parameters proposed in Capello's predictive model [9]

Principal mechanical properties and regression parameters for 42CrMo4				
R_m(MPa)	*HRb*	h_1	h_2	h_3
1000	107	0.011	0.278	0.135

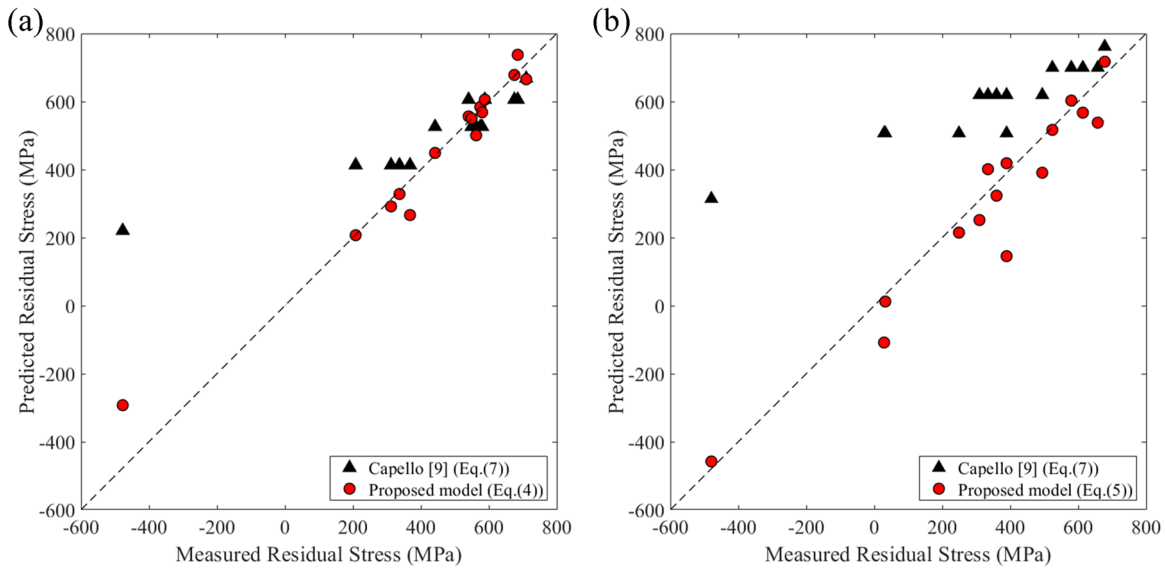

Fig. 18 Comparison of residual stresses estimated by the model proposed in this paper and by Capello's model [9]: **a** for 0.4 mm insert radius and **b** for 0.8 mm insert radius

Table 16 Experimental data

Run	Factor R: insert radius (mm)	Factor a_p: depth of cut (mm)	Factor V_c: cutting speed (m/min)	Factor f_n: feed rate (mm/rev)	Response 1: Ra roughness (µm)	Response 2: residual stresses (MPa)
1	0.4	0.05	138	0.15	0.858	488.4
2	0.4	0.05	138	0.15	1.078	580.3
3	0.4	0.1	107	0.1	0.409	223.2
4	0.4	0.1	107	0.1	0.558	208.3
5	0.4	0.1	107	0.2	1.133	675.3
6	0.4	0.1	107	0.2	1.185	635.4
7	0.4	0.1	169	0.2	1.156	588.2
8	0.4	0.1	169	0.2	1.14	623.5
9	0.4	0.1	169	0.1	0.64	337.2
10	0.4	0.1	169	0.1	0.561	122.3
11	0.4	0.15	76	0.15	0.759	549.3
12	0.4	0.15	76	0.15	0.806	102.5
13	0.4	0.15	138	0.05	0.306	-477.2
14	0.4	0.15	138	0.05	0.657	-513.3
15	0.4	0.15	138	0.15	0.796	141.3
16	0.4	0.15	138	0.15	0.849	562.7
17	0.4	0.15	138	0.15	0.675	553.0
18	0.4	0.15	138	0.15	0.69	421.5
19	0.4	0.15	138	0.15	0.888	461.0
20	0.4	0.15	138	0.15	0.87	610.9
21	0.4	0.15	138	0.25	1.623	710.1
22	0.4	0.15	138	0.25	1.682	702.8
23	0.4	0.15	200	0.15	0.587	441.9
24	0.4	0.15	200	0.15	0.596	363.1
25	0.4	0.2	107	0.1	0.478	312.3
26	0.4	0.2	107	0.1	0.574	314.0
27	0.4	0.2	107	0.2	1.002	519.7
28	0.4	0.2	107	0.2	1.074	685.2
29	0.4	0.2	169	0.2	1.111	508.9
30	0.4	0.2	169	0.2	1.091	540.6
31	0.4	0.2	169	0.1	0.432	357.1
32	0.4	0.2	169	0.1	0.46	368.2
33	0.4	0.25	138	0.15	0.735	597.5
34	0.4	0.25	138	0.15	0.783	575.0
35	0.8	0.05	138	0.15	0.8	334.7
36	0.8	0.05	138	0.15	1.069	496.4

Table 16 (continued)

Run	Factor R: insert radius (mm)	Factor a_p: depth of cut (mm)	Factor V_c: cutting speed (m/min)	Factor f_n: feed rate (mm/rev)	Response 1: Ra roughness (μm)	Response 2: residual stresses (MPa)
37	0.8	0.1	107	0.1	0.477	28.9
38	0.8	0.1	107	0.1	0.551	-253.1
39	0.8	0.1	107	0.2	0.735	657.8
40	0.8	0.1	107	0.2	0.777	439.4
41	0.8	0.1	169	0.2	0.73	514.2
42	0.8	0.1	169	0.2	0.727	613.8
43	0.8	0.1	169	0.1	0.544	249.4
44	0.8	0.1	169	0.1	0.468	253.7
45	0.8	0.15	76	0.15	3.235	133.0
46	0.8	0.15	76	0.15	0.624	309.6
47	0.8	0.15	138	0.05	0.307	-479.3
48	0.8	0.15	138	0.05	0.275	-570.6
49	0.8	0.15	138	0.15	0.488	209.2
50	0.8	0.15	138	0.15	0.555	359.9
51	0.8	0.15	138	0.15	0.406	169.7
52	0.8	0.15	138	0.15	0.41	545.9
53	0.8	0.15	138	0.15	0.475	538.7
54	0.8	0.15	138	0.15	0.565	354.2
55	0.8	0.15	138	0.25	0.854	678.2
56	0.8	0.15	138	0.25	0.902	731.7
57	0.8	0.15	200	0.15	0.711	339.7
58	0.8	0.15	200	0.15	0.6	494.4
69	0.8	0.2	107	0.1	0.385	32.5
60	0.8	0.2	107	0.1	0.461	42.0
61	0.8	0.2	107	0.2	1.259	669.6
62	0.8	0.2	107	0.2	0.693	579.9
63	0.8	0.2	169	0.2	0.445	536.0
64	0.8	0.2	169	0.2	0.466	524.2
65	0.8	0.2	169	0.1	0.54	24.8
66	0.8	0.2	169	0.1	0.372	374.9
67	0.8	0.25	138	0.15	0.367	67.2
68	0.8	0.25	138	0.15	0.535	389.5

Table 17 Expected relative errors for the two roughness (R_a) predictive equations under study

Factor R: insert radius (mm)	Factor a_p: depth of cut (mm)	Factor V_c: cutting speed (m/min)	Factor f_n: feed rate (mm/rev)	Response 1: Ra roughness (μm)	Estimated value (7) (μm)	Relative error (7) (%)	Estimated value ((3) and (4) (μm)	Relative error ((3) and (4)) (%)
0.4	0.05	138	0.15	0.858	1.758	105%	0.964	12%
0.4	0.1	107	0.1	0.409	0.781	91%	0.531	30%
0.4	0.1	107	0.2	1.133	3.125	176%	1.165	3%
0.4	0.1	169	0.2	1.156	3.125	170%	1.196	3%
0.4	0.1	169	0.1	0.64	0.781	22%	0.550	14%
0.4	0.15	76	0.15	0.759	1.758	132%	0.717	6%
0.4	0.15	138	0.05	0.306	0.195	36%	0.298	3%
0.4	0.15	138	0.15	0.675	1.758	160%	0.789	17%
0.4	0.15	138	0.25	1.623	4.883	201%	1.583	2%
0.4	0.15	200	0.15	0.587	1.758	199%	0.642	9%
0.4	0.2	107	0.1	0.478	0.781	63%	0.517	8%
0.4	0.2	107	0.2	1.074	3.125	191%	1.142	6%
0.4	0.2	169	0.2	1.091	3.125	186%	1.013	7%
0.4	0.2	169	0.1	0.46	0.781	70%	0.437	5%
0.4	0.25	138	0.15	0.783	1.758	124%	0.787	1%
0.8	0.05	138	0.15	0.8	0.879	10%	0.735	8%
0.8	0.1	107	0.1	0.477	0.391	18%	0.501	5%
0.8	0.1	107	0.2	0.735	1.563	113%	0.766	4%
0.8	0.1	169	0.2	0.73	1.563	114%	0.780	7%
0.8	0.1	169	0.2	0.727	1.563	115%	0.780	7%
0.8	0.1	169	0.1	0.544	0.391	28%	0.512	6%
0.8	0.15	76	0.15	0.624	0.879	41%	0.689	10%
0.8	0.15	138	0.05	0.307	0.098	68%	0.293	5%
0.8	0.15	138	0.15	0.488	0.879	80%	0.503	3%
0.8	0.15	138	0.25	0.854	2.441	186%	0.769	10%
0.8	0.15	200	0.15	0.711	0.879	24%	0.598	16%
0.8	0.2	107	0.1	0.385	0.391	1%	0.410	7%
0.8	0.2	107	0.2	0.693	1.563	125%	0.651	6%
0.8	0.2	169	0.2	0.445	1.563	251%	0.553	24%
0.8	0.25	138	0.15	0.535	0.879	64%	0.424	21%
0.4	0.05	138	0.15	0.858	1.758	105%	0.964	12%

Table 18 Expected relative errors for the two longitudinal residual stresses predictive equations under study

Factor R: insert radius (mm)	Factor a_p: depth of cut (mm)	Factor V_c: cutting speed (m/min)	Factor f_n: feed rate (mm/rev)	Response 2: residual stresses (MPa)	Estimated value (8) (MPa)	Relative error (8) (%)	Estimated value ((5) and (6) (MPa)	Relative error ((5) and (6)) (%)
0.4	0.05	138	0.15	488.4	525.9	8%	568.5	16%
0.4	0.1	107	0.1	223.2	413.2	85%	207.0	7%
0.4	0.1	107	0.2	675.3	605.9	10%	678.1	0%
0.4	0.1	169	0.2	588.2	605.9	3%	605.6	3%
0.4	0.1	169	0.1	337.2	413.2	23%	328.1	3%
0.4	0.15	76	0.15	549.3	525.9	4%	550.4	0%
0.4	0.15	138	0.05	-477.2	220.5	146%	-292.6	39%
0.4	0.15	138	0.15	553.0	525.9	5%	500.7	9%
0.4	0.15	138	0.25	710.1	667.9	6%	665.3	6%
0.4	0.15	200	0.15	441.9	525.9	19%	449.0	2%
0.4	0.2	107	0.1	312.3	413.2	32%	291.7	7%
0.4	0.2	107	0.2	685.2	605.9	12%	737.3	8%
0.4	0.2	169	0.2	540.6	605.9	12%	556.3	3%
0.4	0.2	169	0.1	368.2	413.2	12%	266.3	28%
0.4	0.25	138	0.15	575.0	525.9	9%	583.9	2%
0.8	0.05	138	0.15	334.7	619.5	85%	401.2	20%
0.8	0.1	107	0.1	28.9	506.8	1653%	-108.4	475%
0.8	0.1	107	0.2	657.8	699.5	6%	537.9	18%
0.8	0.1	169	0.2	514.2	699.5	36%	567.2	10%
0.8	0.1	169	0.2	613.8	699.5	14%	567.2	8%
0.8	0.1	169	0.1	249.4	506.8	103%	214.8	14%
0.8	0.15	76	0.15	309.6	619.5	100%	251.6	19%
0.8	0.15	138	0.05	-479.3	314.1	166%	-458.0	4%
0.8	0.15	138	0.15	209.2	619.5	196%	323.3	55%
0.8	0.15	138	0.25	678.2	761.5	12%	717.0	6%
0.8	0.15	200	0.15	339.7	619.5	82%	390.7	15%
0.8	0.2	107	0.1	32.5	506.8	1458%	12.1	63%
0.8	0.2	107	0.2	579.9	699.5	21%	602.9	4%
0.8	0.2	169	0.2	536.0	699.5	30%	516.6	4%
0.8	0.25	138	0.15	389.5	619.5	59%	418.5	7%

Acknowledgements Diego Díaz-Salamanca and Miguel Muñiz-Calvente thank the University of Oviedo for the financial support received through the UNOV-22-RLD-UE-5 project. Pejman Ebrahimzadeh and Inés Fernández-Pariente thank the Spanish Government for the financial support received for the research project TED2021-130306B-100. Iñigo Llavori, Alaitz Zabala, and Miren Larrañaga are grateful for the support received from the Spanish Government within the HYBRID project (PID2021-124245OA-I00) and the financial support from the Government of the Basque Country for the development of the STEINER project (PIBA 2023/1/0052). Jan Papuga gratefully acknowledges the support of the Czech Science Foundation within the project 23-06130K.

Author contribution Diego Díaz Salamanca: conceptualization, methodology, data curation, formal analysis, validation, writing—original draft, and writing—review and editing. Miguel Muñiz Calvente: conceptualization, methodology, resources, funding acquisition, data curation, formal analysis, validation, supervision, project administration, and writing—review and editing. Pejman Ebrahimzadeh: conceptualization, methodology, data curation, formal analysis, validation, and writing—review and editing. Iñigo LLavori: conceptualization, methodology, resources, funding acquisition, data curation, formal analysis, validation, and writing—review and editing. Alaitz Zabala: conceptualization, methodology, resources, funding acquisition, data curation, formal analysis, validation, and writing—review and editing. Pablo Pando: resources, funding acquisition, investigation, and writing—review and editing. Carlos Suárez Álvarez: conceptualization, methodology, data curation, and writing—review and editing. Inés Fernández Pariente: conceptualization, methodology, data curation, formal analysis, validation, and writing—review and editing. Miren Larrañaga: conceptualization, methodology, resources, funding acquisition, data curation, formal analysis, validation, and writing—review and editing. Jan Papuga: conceptualization, methodology, resources, funding acquisition, validation, and writing—review and editing.

Funding Open Access funding provided thanks to the CRUE-CSIC agreement with Springer Nature. This work was supported by the University of Oviedo [UNOV-22-RLD-UE-5]; the Government of the Basque Country, Spain [PIBA 2023/1/0052]; the Spanish Government

[TED2021-130306B-100 and PID2021-124245OA-I00]; and the Czech Science Foundation [23-06130 K].

Declarations

Competing interests The authors declare no competing interests.

Open Access This article is licensed under a Creative Commons Attribution 4.0 International License, which permits use, sharing, adaptation, distribution and reproduction in any medium or format, as long as you give appropriate credit to the original author(s) and the source, provide a link to the Creative Commons licence, and indicate if changes were made. The images or other third party material in this article are included in the article's Creative Commons licence, unless indicated otherwise in a credit line to the material. If material is not included in the article's Creative Commons licence and your intended use is not permitted by statutory regulation or exceeds the permitted use, you will need to obtain permission directly from the copyright holder. To view a copy of this licence, visit http://creativecommons.org/licenses/by/4.0/.

References

1. DIN 50100:2016–12 (2016) Load controlled fatigue testing - execution and evaluation of cyclic tests at constant load amplitudes on metallic specimens and components. Deutsches Institut für Normung, Berlin, Germany
2. ASTM E466–15 (2015) Standard practice for conducting force controlled constant amplitude axial fatigue tests of metallic materials. American Society for Testing and Materials, West Conshohocken, USA
3. ISO 1099:2017 (2017) Metallic materials — fatigue testing — axial force-controlled method. International Organisation for Standarizatation, Geneva, Switzerland
4. Minamizawa K et al (2022) Fatigue limit estimation for carburized steels with surface compressive residual stress considering residual stress relaxation. Int J Fatigue 160:106846
5. Withers PJ, Bhadeshia HKDH (2001) Residual stress part 2 - nature and origins. Mater Sci Technol 17(4):366–375
6. Elsheikh AH et al (2022) A comprehensive review on residual stresses in turning. Adv Manuf 10(2):287–312
7. Bassanini G, Bisi A, Capello E (1999) Residual Stresses and Surface Roughness in Turning. J Eng Mater Technol 121(3):346–351
8. Capello E (2005) Residual stresses in turning: part I: influence of process parameters. J Mater Process Technol 160(2):221–228
9. Capello E (2006) Residual stresses in turning: part II influence of the machined material. J Mater Process Technol 172(3):319–326
10. Arola D, Williams CL (2002) Estimating the fatigue stress concentration factor of machined surfaces. Int J Fatigue 24(9):923–930
11. Javidi A, Rieger U, Eichlseder W (2008) The effect of machining on the surface integrity and fatigue life. Int J Fatigue 30(10–11):2050–2055
12. Asiltürk I, Çunkaş M (2011) Modeling and prediction of surface roughness in turning operations using artificial neural network and multiple regression method. Expert Syst Appl 38(5):5826–5832
13. Saini S, Ahuja IS, Sharma VS (2012) Residual stresses, surface roughness, and tool wear in hard turning: a comprehensive review. Mater Manuf Process 27(6):583–598
14. Panzadaras CN, Davim JP, and Petropoulos GP (2008) Surface texture characterization and evaluation related to machining. In: Davim JP (ed) Surface Integrity in Machining, Springer, pp 37–66
15. Field M, Kakles J, Cammett J (2005) A Review of Measuring Methods for Surface Integrity. Metcut Research Associates Inc, Ohio
16. Fathi J, Ebrahimzadeh P, Farasati R, Teimouri R (2019) Friction stir welding of aluminum 6061–T6 in presence of watercooling: analyzing mechanical properties and residual stress distribution. Int J Light Mater Manuf 2(2):107–115
17. Farasati R, Ebrahimzadeh P, Fathi J, Teimouri R (2019) Optimization of laser micromachining of Ti–6Al–4V. Int J Light Mater Manuf 2(4):305–317
18. Santhosh AJ, Tura AD, Jiregna IT, Gemechu WF, Ashok N, Ponnusamy M (2021) Optimization of CNC turning parameters using face centred CCD approach in RSM and ANN-genetic algorithm for AISI 4340 alloy steel. Results Eng 11:100251
19. Zhu Z, Lu Y, Xie Q, Li D, Gao N (2017) Mechanical properties and dynamic constitutive model of 42CrMo steel. Mater Des 119:171–179
20. Bartošák M, Horváth J, Španiel M (2020) Isothermal low-cycle fatigue and fatigue-creep of a 42CrMo4 steel. Int J Fatigue 135:105538
21. Papuga J, Mžourek M, Matušů M, Mára V, Čapek J (2023) Investigation of the size effect on 42CrMo4 + QT steel in the high-cycle fatigue domain part I: Experimental campaign. Int J Fatigue 175:107743
22. Noordin MY, Venkatesh VC, Sharif S, Elting S, Abdullah A (2004) Application of response surface methodology in describing the performance of coated carbide tools when turning AISI 1045 steel. J Mater Process Technol 145(1):46–58
23. Lalwani DI, Mehta NK, Jain PK (2008) Experimental investigations of cutting parameters influence on cutting forces and surface roughness in finish hard turning of MDN250 steel. J Mater Process Technol 206(1–3):167–179
24. Öktem H, Erzurumlu T, Kurtaran H (2005) Application of response surface methodology in the optimization of cutting conditions for surface roughness. J Mater Process Technol 170(1–2):11–16
25. Ebrahimzadeh P, Martínez LBP, Pariente IF, Varela FJB (2024) Optimization of shot-peening parameters for steel AISI 316L via response surface methodology (RSM): introducing two novel mechanical aspects. Int J Adv Manuf Technol 132:647–667
26. Fitzpatrick ME et al (2010) Determination of residual stresses by X-ray diffraction - Issue 2. Measurement Good Practice Guide (52)
27. Lange DA, Jennings HM, Shah SP (1993) Analysis of surface roughness using confocal microscopy. J Mater Sci 28(14):3879–3884
28. UNE-EN ISO 21920–3 (2023) Geometrical product specifications (GPS) -Surface texture : Profile. International Organisation for Standarizatation. UNE: Madrid, Spain
29. Anderson MJ and Whitcomb PJ (2003) How to use graphs to diagnose and deal with bad experimental data. Stat-Ease Inc, Minneapolis
30. Weisberg S (2014) Applied linear regression, 4th edn. Wiley, New York
31. Box G, Stuart J, Hunter W (2005) Statistics for experimenters. Wiley, New York

Publisher's Note Springer Nature remains neutral with regard to jurisdictional claims in published maps and institutional affiliations.